Linear theory of the spatial signatures of critical slowing down

Giulio Tirabassi*
Universitat Politècnica de Catalunya, Departament de Fisica, Rambla Sant Nebridi 22, Terrassa 08222, Barcelona, Spain

(Received 19 January 2024; accepted 26 April 2024; published 3 June 2024)

Critical slowing down is considered one of the main signs that a dynamical system is close to a tipping point. For this reason, early-warning indicators have been developed to identify it, mainly based on the temporal evolution of the system under analysis. Yet, it has been shown that critical slowing down also displays spatial signatures, such as an increase in the spatial correlation. However, these signatures are based only on heuristic observations and the analysis of numerical simulations and do not have a sound theoretical foundation. In this work I will derive analytical expressions for typical spatial early-warning indicators of critical transitions in spatially extended systems, such as spatial correlation, spatial variance, and spatial permutation entropy, in the linearized limit. As a result, I will show that the common belief that the spatial correlation increases when a bifurcation is imminent is false. Other indicators, instead, might represent more robust alternatives, such as the spatial permutation entropy or the spatial variance.

DOI: 10.1103/PhysRevResearch.6.023228

I. INTRODUCTION

Tipping points are often modeled as bifurcations of some dynamical systems [1]. Usually the bifurcation is of "catastrophic" type, in which a stable fix point disappears or loses stability and the system experiences an abrupt excursion towards a new stable state. Therefore, understanding whether a system is close to tip is paramount in real-life applications [2–5] and is still an unresolved problem [6].

One of the main characteristics of a dynamical system close to any local bifurcation is the so-called "critical slowing down" (CSD) [7]. As a dynamical system approaches a critical point, it starts showing changes in its response to perturbations, typically manifesting as an increase in the time required to return to equilibrium.

The CSD can be detected directly from time-series data, and it usually manifests as an increase in the temporal autocorrelation or in the time-series variance [7]. Several studies have reported signatures of CSD in very diverse fields of applications, such as ecology [5,8], climate [9,10], sociology [11], and finance [12], just to name a few.

The CSD, however, is not only a temporal feature but also implies spatial effects [7,8,13], especially in spatially extended systems such as ecosystems and climate systems [14–16]. Therefore, recognizing the spatial signatures associated with CSD is crucial in managing critical transitions in fields that strongly impact human activities such as desertification or forest loss.

Popular spatial signatures of the CSD are spatial correlation [13,17], spatial variance [17,18], and spatial skewness [18]. These indicators are easy to compute and have been shown to be effective in different kinds of bifurcations, such as the Turing bifurcation [17]. Spatial indicators also have the advantage that to be computed they require the measurement of the system's state at a given time, whereas temporal indicators are based on the analysis of a time series, which might be problematic for those systems where the characteristic timescale is particularly long, such as vegetation dynamics.

These indicators have been tested mainly in models and have been applied scarcely in real datasets [16,19]. Indeed, recently the spatial correlation was shown to be relatively poor when predicting tipping points in real-world tree-cover data [20], underperforming with respect to a nonlinear indicator such as the spatial permutation entropy.

All these indicators are mainly based on the heuristic idea that at the bifurcation point, spatial interactions dominate the dynamics, increasing the spatial coherence of the system. However, there has been no attempt to rigorously justify this intuition. In this work I want to draw closed-form formulas for the spatial correlation, variance, and permutation entropy for reaction-diffusion systems, often employed to model spatially extended tipping systems, particularly in ecological applications [13,14,18,21,22]. From these calculations I aim to see how general the behavior of the indicators is close to a local bifurcation and therefore how reliable they can be as early-warning indicators of tipping points in reaction-diffusion systems.

In particular, I will show that contrary to the common belief [13,17], the spatial correlation can increase as well as decrease when approaching a bifurcation point, whereas the spatial permutation entropy seems to have a more robust behavior, decreasing close to the critical point. However, despite being general, depending on the system parameters this tendency can be extremely weak and could be easily hidden by noise in real-world applications.

*giulio.tirabassi@upc.edu

Published by the American Physical Society under the terms of the Creative Commons Attribution 4.0 International license. Further distribution of this work must maintain attribution to the author(s) and the published article's title, journal citation, and DOI.

II. RESULTS

The main object of study will be reaction-diffusion systems described by the following evolution equation:

$$\dot{\mathbf{u}} = \mathbf{F}(\mathbf{u}) + \mu\Delta\mathbf{u} + \sigma\boldsymbol{\xi}. \tag{1}$$

Here, $\mathbf{u}(t,\mathbf{r})$ represents a $\mathbb{R}^{n+1} \to \mathbb{R}^m$ vector function, Δ denotes the n-dimensional Laplacian operator, and μ stands for the diffusion coefficient. The vector field $\mathbf{F}$ represents the reaction component of the system, and it is a $\mathbb{R}^m \to \mathbb{R}^m$ vector field. Assuming the existence of a stable fix point $\bar{\mathbf{u}}$ such that $\mathbf{F}(\bar{\mathbf{u}}) = 0$, the deterministic part of Eq. (1) admits a homogeneous stationary solution $\mathbf{u}(t,\mathbf{r}) = \bar{\mathbf{u}}$. Finally, the system is perturbed by a white-noise term of variance σ^2, which is decorrelated both in time and space.

The numerical integration of Eq. (2) often involves discretizing the position vector $\mathbf{r}$ on a regular lattice with step size h. This discretization formally transforms the equation into a network of identical subsystems evolving according to the reaction term and interacting linearly on a regular lattice of N nodes:

$$\dot{\mathbf{u}}_k = \mathbf{F}(\mathbf{u}_k) + \nu\sum_{j\in\mathcal{N}_k}(\mathbf{u}_j - \mathbf{u}_k) + \sigma\boldsymbol{\xi}_k. \tag{2}$$

Here, $\mathbf{u}_k = \mathbf{u}(t,\mathbf{r}_k)$, $\mathcal{N}_k$ represents the lattice neighbors of node k, and ν is a lattice diffusion coefficient, a parameter of order μh^{-2}. In this lattice representation the homogeneous and stationary solution corresponds to $\mathbf{u}_k = \bar{\mathbf{u}}\ \forall k$.

In the case of $\sigma > 0$, the stationarity and stability of the homogenous solution should be treated in a statistical sense. In particular, one can investigate the stationarity of the probability distribution of the values of $\mathbf{u}_k$.

A. Unidimensional systems

The case $m = 1$ is straightforward to treat by associating to the Langevin equation (2) a corresponding Fokker-Plank equation [23]:

$$\frac{\partial p(u_k)}{\partial t} = -\sum_{i=1}^{N}\frac{\partial}{\partial u_i}(G(u_k)\,p(u_k)) + \frac{\sigma^2}{2}\sum_{i=1}^{N}\frac{\partial^2 p(u_k)}{\partial u_i^2}, \tag{3}$$

where $G(u_k) = F(u_k) + \nu\sum_{j\in\mathcal{N}_k}(u_j - u_k)$.

It is well known that if the reaction term can be expressed as the gradient of a potential function $V(u)$, the stationary solution of Eq. (3) can be found explicitly:

$$p(u_k) \propto \exp\left\{-\frac{2}{\sigma^2}U(u_k)\right\}, \tag{4}$$

where $U = V + \frac{\nu}{2}\sum_i u_i\sum_j L_{ij}u_j$. This result is valid if U represents a potential well that approaches infinity quickly enough.

The probability $p(u_k)$ enables the calculation of the typical slowing-down signatures, such as the variance and the spatial correlation, which is simply the covariance between neighboring nodes normalized by the variance. However, for a general U, analytical calculations of such indicators might be unfeasible, and one has to rely on numerical calculations.

It is possible to overcome this difficulty, considering that if the noise term is sufficiently small and the system is around the potential minimum represented by the fix point $\bar{u}$, the likelihood of the escape from the potential well will be small and one can consider the system confined around the fix point for every practical application. Without loss of generality, one can choose $\bar{u} = 0$.

Linearizing the system transforms the probability distribution p to a multivariate Gaussian with the following covariance matrix:

$$\boldsymbol{\Sigma} = \frac{\sigma^2}{2}(\nu\mathbf{L} - \mathbf{J})^{-1}. \tag{5}$$

For $m = 1$, the Jacobian of the reaction part simplifies to $\mathbf{J} = -\lambda\mathbf{I}$ with $\lambda > 0$ and $\mathbf{I}$ is the identity matrix. Therefore, the covariance matrix can be explicitly expressed as

$$\Sigma_{ij} = \sum_{k=1}^{N} e_k^i\frac{1}{\nu\Lambda_k + \lambda}e_k^j, \tag{6}$$

where $\mathbf{e}_k$ and Λ_k are the eigenvectors and eigenvalues of the Laplacian matrix, respectively. This result holds for a generic Laplacian matrix; however, in the case of a circulant matrix, such as a regular lattice, the calculation of the eigenvalues and the eigenvectors can be done explicitly [24]. In particular, in the case of a ring we will have

$$\Sigma_{ij} = \frac{\sigma^2}{2}\frac{1}{N\nu}\sum_{k=0}^{N-1}\frac{\cos\left[2\pi(i-j)\frac{k}{N}\right]}{2 - 2\cos\left(2\pi\frac{k}{N}\right) + \lambda/\nu}. \tag{7}$$

The generalization of this formula to two- and three-dimensional (2D, 3D) regular lattices is straightforward.

Considering that in applications N is usually a large number, the expression can be simplified by approximating the series with the corresponding integral. In this case the spatial correlation can be written as

$$\mathrm{SC} = \frac{\Sigma_{10}}{\Sigma_{00}} \approx 1 - \frac{1}{2}\sqrt{\frac{\lambda}{\nu}}\left(\sqrt{\frac{\lambda}{\nu} + 4} - \sqrt{\frac{\lambda}{\nu}}\right). \tag{8}$$

From this simplified formula, it is clear that the spatial correlation depends only on the ratio between λ and ν, and it is bounded between 0 and 1, that is, it cannot take negative values.

If the dynamical system represented by F undergoes a bifurcation, the constant $-\lambda$, which is the eigenvalue of the Jacobian matrix of multiplicity N, will go to zero. Then the spatial correlation will increase from values close to 0 for $\lambda \gg \nu$, approaching 1 in the limit $\lambda \to 0$.

The multivariate Gaussian distribution allows the explicit calculation of additional quantities, such as the spatial permutation entropy [25]. For ordinal patterns of three nodes on the ring, the entropy is given by

$$H = -2P\log(P) - (1-2P)\log\left(\frac{1-2P}{4}\right), \tag{9}$$

where

$$P = \frac{1}{4} + \frac{1}{2\pi}\arcsin\left(\frac{\Sigma_{01} - \frac{1}{2}(\Sigma_{00} + \Sigma_{02})}{\Sigma_{00} - \Sigma_{01}}\right) \tag{10}$$

is computed from the orthant probabilities of a multivariate normal. Hence, it is clear that the covariance matrix

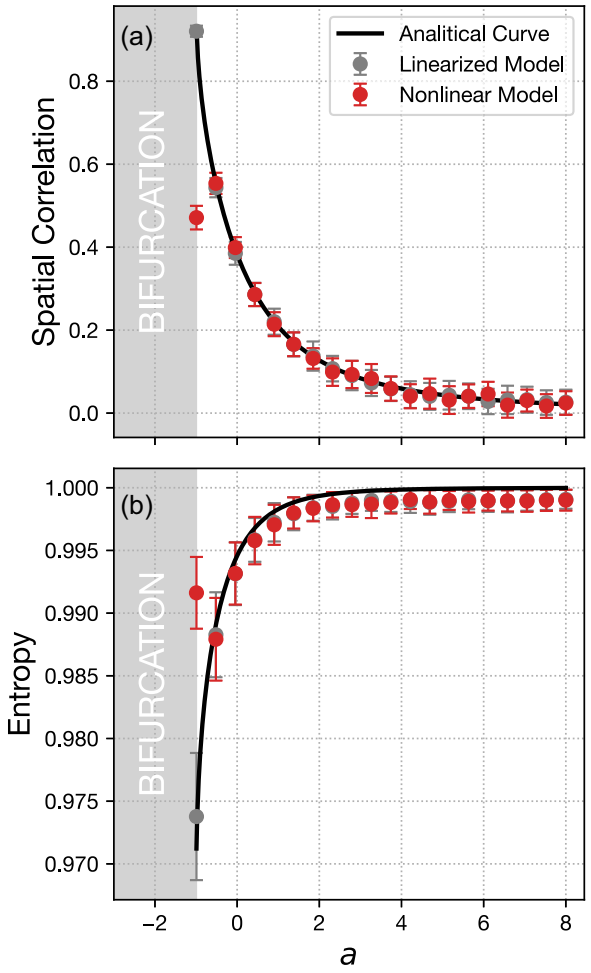

FIG. 1. Spatial correlation (a) and normalized spatial permutation entropy (b) of a unidimensional reaction-diffusion model whose homogeneous state undergoes a transcritical bifurcation as a function of the bifurcation parameter a (see text for details). For the sake of clarity, the entropy is normalized between 0 and 1. The dots represent the average obtained by analyzing 1000 time steps sampled every 100 integration steps. The results for the full nonlinear model are reported in red; in gray are the results for the linearized model. The solid black line represents the analytical results computed via Eqs. (8) and (9).

completely encodes the information about the entropy. Details on the derivation of these formulas are provided in the Appendixes.

In the same limit of Eq. (8), it can be seen that P is bounded between $\frac{1}{6}$ and $\frac{1}{4}$, which in turn bounds the entropy between $\log(6)$ for $\lambda \gg \nu$ and $\frac{5}{2}\log(2)$ for $\lambda \to 0$, a 3% difference. Therefore eventual entropy variations due to the occurrence of a bifurcation at $\lambda \to 0$ will need a large number of spatial samples to be robustly assessed. Finally, it can be seen that the decrease towards $\lambda = 0$ is monotonous.

These analytical calculations can be validated through simulations of Eq. (2). As an example I considered the following form for the reaction term $F(u) = -u^3 - au^2 + u(1 + a)$, which has three fix points, $u = \{0, 1, -1 - a\}$, and two transcritical bifurcations for $a = \{-1, -2\}$, which acts as a bifurcation parameter. The results are reported in Fig. 1 for a decreasing down to -1 and the stable fix point $\bar{u} = -1 - a$ colliding with the unstable fix point at $u = 0$. A perfect agreement between the analysis and the linearized model can be observed. The nonlinear model, instead, follows the prediction up to the last point tested, where the noise level kicks the system out of the shrunk basin of attraction of $\bar{u}$.

B. Two-dimensional system and spatial correlation decrease

I now consider $m = 2$ and a linearized system for the variable $\mathbf{u} = (u, v)$. Again, I consider the system dynamics around a stable fix point, and without loss of generality, I take it to be $\bar{\mathbf{u}} = 0$. The Jacobian of the reaction term, in this case, will be given by a $2N \times 2N$ square matrix of the form

$$\mathbf{J} = \begin{pmatrix} a\mathbf{I} & b\mathbf{I} \\ c\mathbf{I} & d\mathbf{I} \end{pmatrix}, \tag{11}$$

where a, b, c, and d are four constants.

In the most general case, there will be two different diffusion coefficients for the two components of $\mathbf{u}$, and the $2N \times 2N$ evolution matrix will be a block-diagonal matrix of the form

$$\mathbf{A} = \begin{pmatrix} a\mathbf{I} - \nu_1\mathbf{L} & b\mathbf{I} \\ c\mathbf{I} & d\mathbf{I} - \nu_2\mathbf{L} \end{pmatrix}. \tag{12}$$

As for the one-dimensional (1D) case, one can exploit the presence of identity matrices to work in the Laplacian eigenvectors base. In this base it is easy to see that $\mathbf{A}$ is stable if $a + d - \nu_1\Lambda_k - \nu_2\Lambda_k < 0$ and $ad - cb + \Lambda_k(\nu_2 a + \nu_1 d) + \nu_1\nu_2\Lambda_k^2 > 0$. For the zero eigenvalue of the Laplacian matrix, $\Lambda_0 = 0$, these conditions represent the instabilities of the dynamical system $\mathbf{F}$, while the instabilities related to $\Lambda_k > 0$ will be the Turing bifurcations of the spatial mode k associated with the Laplacian eigenvector $\mathbf{e}_k$.

The Langevin equation generated by the matrix $\mathbf{A}$ can be associated with a Fokker-Plank equation that admits a stationary solution [23]. If the fix-point $\bar{\mathbf{u}}$ is stable, $\mathbf{A}$ is contractive and the stationary solution of the Fokker-Plank equation is an attractor for the probability distributions of $\mathbf{u}_k$.

Moreover, the stationary solution will be a multivariate Gaussian, whose covariance matrix can be obtained as the matrix $\mathbf{\Sigma}$ solving the Lyapunov continuous-time equation $\mathbf{A\Sigma} + \mathbf{\Sigma A}^T = -\sigma^2\mathbf{I}$, which gives the following expression for the covariance in the u subspace:

$$\Sigma_{ij} = -\frac{\sigma^2}{2N}\sum_k e_k^i e_k^j \frac{d_k(a_k + d_k) + b(b + c)}{(a_k + d_k)(a_k d_k - bc)}, \tag{13}$$

where $a_k = a - \nu_1\Lambda_k$ and $d_k = d - \nu_2\Lambda_k$. The derivation of this formula is provided in the Appendixes.

Equation (13) can be used to compute the spatial correlation and the spatial permutation entropy using Eqs. (8) and (9). The case of the spatial correlation is particularly interesting and is reported in Fig. 2(a), as a function of the parameters a and ν_1. As it can be seen, the spatial correlation displays a quadrupolar structure. In particular, it increases towards the $a = -d$ and $a = bc/d$ instability boundaries, while it decreases when approaching a great part of the boundary that marks the Turing instability. From Fig. 2 it is clear that this decrease corresponds to the highest modes giving rise to the instability, that is, modes at high wave number. Intuitively, we might interpret this feature by thinking that just before

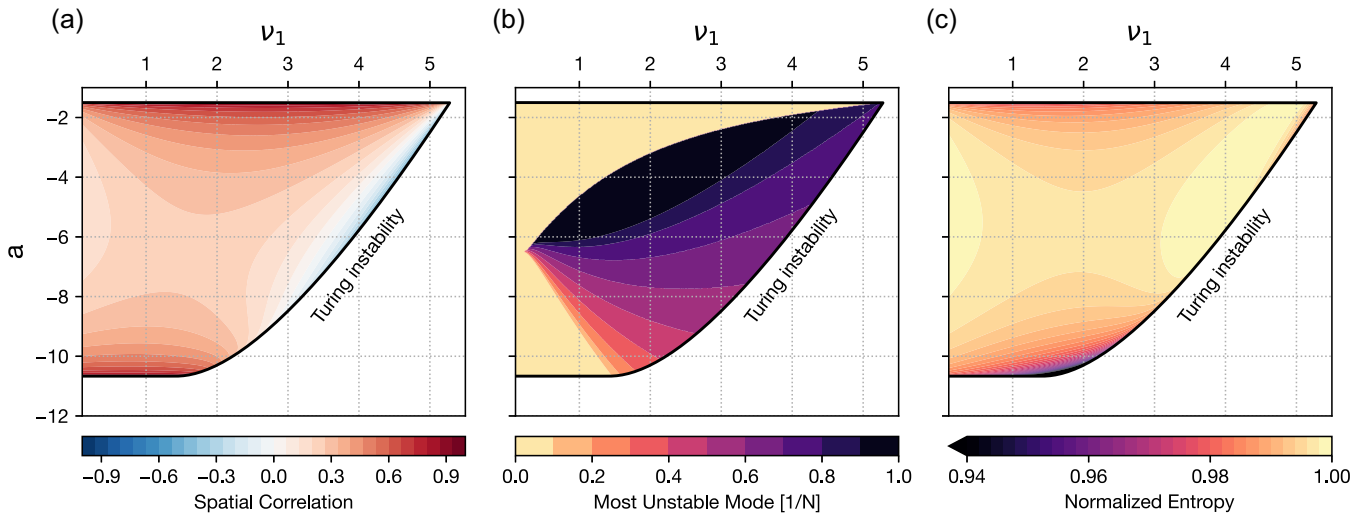

FIG. 2. (a) Spatial correlation for the reaction-diffusion system of Eq. (C3) as a function of a and ν_1. In this example, the rest of the parameters are $b = -c = -4$, $d = \frac{3}{2}$, $\nu_2 = \frac{1}{5}$. The solid black line separates the stable and unstable regions of the parameter space. (b) Order of the most unstable mode of **A**. Higher orders are associated to high spatial wave number. Zero-mode instabilities correspond to instability of the Jacobian matrix **J**. (c) As in (a), but for the normalized spatial permutation entropy of ordinal patterns of three consecutive nodes.

the bifurcation the most unstable mode will start emerging, stimulated by the noise, being the one that relaxes the slowest back to equilibrium. The high wave number means fast spatial oscillations entailing low, even negative correlation between neighbors.

The entropy is reported in Fig. 2(c). As the spatial correlation, it displays a quadrupolar structure, with the notable difference that it always decreases close to the bifurcation boundary. Nevertheless, for the medium to high Turing wave numbers, the decrease in entropy close to the instability is minimal and confined to a very narrow range of parameter values. Therefore, in this condition it might be challenging to observe experimentally.

In Fig. 3 results from simulations of Eq. (2) confirm the predicted drop in spatial correlation, providing additional validation for the analytical calculations. It is also possible to appreciate the small flexion in the normalized spatial permutation entropy; however, the variation is well below the temporal variance of the measure. Moreover, being so close to 1, the normalized entropy is significantly affected by the negative bias of the estimator. Such a bias can be reduced by considering all the time steps to compute the symbols' probability, instead of computing the entropy at each time step and then averaging. Such a procedure is commonly known as "pooling" [26].

III. DISCUSSION

The increase of spatial correlation is considered to be one of the main spatial signatures of critical slowing down, and therefore of a forthcoming tipping point [13]. I proved this to be true when analyzing reaction-diffusion models of a single scalar field. In this case, according to Eq. (8), the spatial correlation steadily increases towards the bifurcation as a power law of the ratio between the reaction and diffusion timescales. The formula is computed using a 1D lattice, but the extension to 2D and 3D lattices is straightforward.

I have also shown that the rise in spatial correlation is linked to a decrease in entropy, as the latter is determined by the coefficients of the covariance matrix. Passing from scalar to vectorial fields drastically changes the results, at least for the spatial correlation. In particular, from the calculation it is evident that the assumption holding so far that an increase in the spatial correlation would be a robust indicator of critical slowing down is no longer correct.

In previous studies [14] it was shown that the spatial correlation increases not only on bifurcations that are proper of the dynamical system **F**, in which the diffusion plays a secondary role, but also on the Turing bifurcations, which are made possible by the presence of diffusion. Here, I have shown that this is not generally true. When the system undergoes a Turing bifurcation at mid to high spatial wave number, the spatial correlation decreases up to the point where it reaches negative values.

On the contrary, the entropy decreases towards each bifurcation point. In the zero-mode bifurcations, the mechanisms are the same as for the scalar field, so we expect and indeed find the same behavior. For the Turing bifurcation, instead, the entropy is able to capture the seeds of the spatial structures that would fully emerge from the background noise once the bifurcation point is reached.

However, the entropy decrease happens at different rates and by different amounts, up to the point in which it might become difficult to detect experimentally. In these cases the observed behavior might be a rise of the entropy, followed by a relatively stable plateau, and the bifurcation would happen in a state very close to the maximum possible entropy. Therefore, the absolute value of the entropy cannot be used as an early-warning indicator of a forthcoming transition, and the trend can be tricky to interpret, as it might be too weak to be robustly detected.

The spatial variance, Σ_{00}, could represent a more robust indicator. This quantity diverges approaching the bifurcation, both in the $m = 1$ case and in the $m = 2$ case. In the latter the

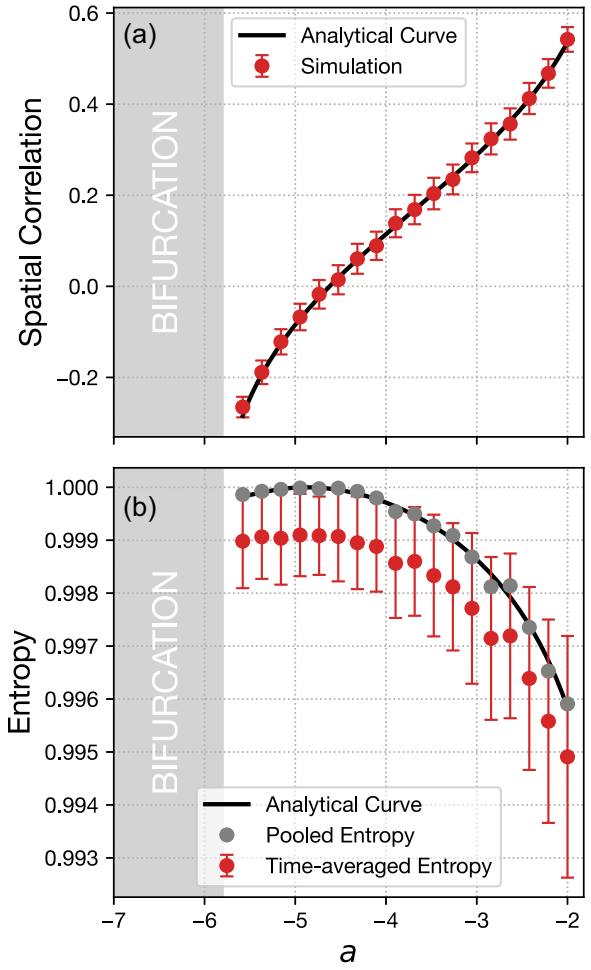

FIG. 3. Spatial correlation (a) and spatial permutation entropy (b) for the reaction-diffusion model of Fig. 2 for $\nu_1 = 4$. For clarity the entropy is normalized between 0 and 1. The red dots represent the average obtained by analyzing 1000 time steps sampled every 100 integration steps of a ring of 100 nodes. The gray dots in (b) represent the spatial permutation entropy computed using all the time steps to compute the symbols statistics, rather than computing the entropy at each time step and averaging afterward, a technique known as "pooling."

increase is generalized, as it is related to the fact that if mode k loses stability, then $a_k + d_k$ changes sign, being 0 at the bifurcation. Hence, Eq. (13) would have a diverging element in the sum. Moreover, the spatial variance is a robust indicator also in the case of a generic Laplacian connectivity, i.e., the case in which the identical systems of the discretized equation, Eq. (2), are interacting on a network (see the Appendixes).

These results suggest that the usage of only one indicator to monitor the arrival of a bifurcation can be insufficient in the case of spatial indicators, and a general approach in which multiple indicators are tracked not only might be able to foresee the arrival of a bifurcation, but also to draw some information about the nature of the bifurcation itself. For example, a combination of a decreasing spatial correlation, increasing variance, and increasing entropy can indicate the arrival of a bifurcation, but the fact that the entropy increases is an indication that the bifurcation is not imminent, as it would have to plateau first, or even decrease. The decreasing spatial correlation, moreover, would indicate that a high-wave-number spatial mode is the one that will likely be the cause of the instability. Another possible spatial indicator, which recently was proven to be an effective early-warning indicator of catastrophic shifts of tree populations, is provided by the diagonal elements of the precision matrix, that is, the inverse of the covariance matrix [27]. In the case considered here, for $m = 2$ it would be the square matrix given by the four elements Σ_{00}, Σ_{0N}, Σ_{N0}, and Σ_{NN}. While Σ_{00} can be obtained by Eq. (13), the other three elements can be derived by extending the equation to the other subspaces, u-v and v. Therefore, this indicator is linked to the fields' variance, but for the tree species tested by the authors, it provides a sharper signal than the simple raise in the variance [27].

ACKNOWLEDGMENTS

The author would like to acknowledge the support of Ministerio de Ciencia e Innovación, Spain, Project No. PID2021-123994NB-C21.

APPENDIX A: SPATIAL PERMUTATION ENTROPY CALCULATION FOR A MULTIVARIATE GAUSSIAN VARIABLE

This section will provide more details on the calculation of Eqs. (10) and (11) of the main manuscript. We start by considering the vectorial variable $\mathbf{u} \in \mathbb{R}^N$ distributed as a multivariate Gaussian of zero mean and covariance matrix $\mathbf{\Sigma}$. In the case of the main manuscript, each element of the vector represents the value of the field u on a certain node.

To compute the permutation entropy of a sample of $\mathbf{u}$ we have first to convert the vector into a series of ordinal patterns [28]. To do so we divide the vector into segments of length Q. Then each value within the segment is assigned a symbol according to the ranking of the values inside each segment. The ordinal patterns take into account the local variations of the field u rather than its amplitude.

For example, if $Q = 3$, as in the main manuscript, and $u_k < u_{k+1} < u_{k+2}$, the u_k value is replaced by the ordinal pattern "012," while if $u_k > u_{k+1} > u_{k+2}$, the u_k the pattern "210" is used instead, and so forth. Considering patterns of length Q there are $Q!$ different possible patterns. An example is depicted in Fig. 4.

Once the values have been translated into a set of symbols, the occurrence probabilities of these symbols, p_s, give the normalized permutation entropy of $\mathbf{u}$ as

$$H = -\frac{1}{\log(Q!)} \sum_{s}^{Q!} p_s \log(p_s), \tag{A1}$$

which is a number normalized between 0 and 1. These occurrence probabilities can be computed explicitly in the case of the main manuscript. First of all, given the homogeneity and the isotropy of the systems studied in the main manuscript, $p_{012} = p_{210}$ and $p_{120} = p_{021} = p_{201} = p_{102}$, which together with (A1) gives Eq. (10) of the main manuscript.

Therefore, to determine H it is sufficient to compute $P = p_{012}$. To do so we leverage the fact that if the various

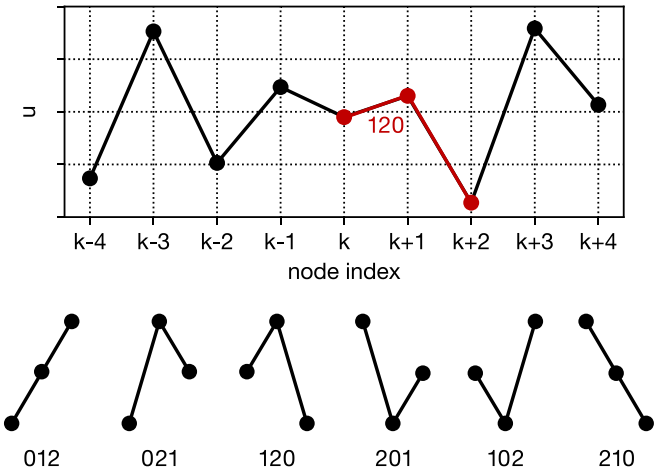

FIG. 4. Example of ordinal pattern construction for node k using $Q = 3$.

u_k are Gaussian, $z_k = u_k - u_{k+1}$ and $z_{k+1} = u_{k+1} - u_{k+2}$ are Gaussian too. Therefore, the probability of the symbol 012 is equivalent to the probability of having both z_k and z_{k+1} negative. Noting that the joint probability of z_k and $z_k + 1$ is a bivariate Gaussian, these probabilities can be computed as its orthant probability:

$$P = \frac{1}{4} + \frac{1}{2\pi} \arcsin(\rho), \tag{A2}$$

where ρ is the correlation between z_k and z_{k+1}, which can be computed using the covariance between z_k and z_{k+1} that is inherited by the covariance between the u_k:

$$\rho = \frac{\mathrm{Cov}(z_k, z_{k+1})}{\mathrm{Var}(z_k)\mathrm{Var}(z_{k+1})} = \frac{\Sigma_{01} - \frac{1}{2}(\Sigma_{00} + \Sigma_{02})}{\Sigma_{00} - \Sigma_{01}}. \tag{A3}$$

Generalizing these formulas to ordinal patterns of higher order is lengthy but straightforward.

We can compute an explicit form of ρ in function of the system parameters for $m = 1$. We use Eq. (8) of the main manuscript taking the limit $N \to \infty$, which is converting the sum into an integral. In this case,

$$\rho = \frac{1}{4}\sqrt{\frac{\lambda}{\nu}}\left(\sqrt{\frac{\lambda}{\nu} + 4} - \sqrt{\frac{\lambda}{\nu}}\right), \tag{A4}$$

which is bounded between $\frac{1}{2}$ and 0 for $\lambda \to \infty$ and $\lambda \to 0$, respectively. Consequently, H is bounded between $\frac{5}{2}\log(2)$ and 1, as stated in the main manuscript.

APPENDIX B: SOLUTION OF THE CONTINUOUS-TIME LYAPUNOV EQUATION

This section provides more details on the calculation necessary to arrive at Eq. (14) of the main manuscript, which is to solve the equation $\mathbf{A}\boldsymbol{\Sigma} + \boldsymbol{\Sigma}\mathbf{A}^T = -\sigma^2\mathbf{I}$, where

$$\mathbf{A} = \begin{pmatrix} a\mathbf{I} - \nu_1\mathbf{L} & b\mathbf{I} \\ c\mathbf{I} & d\mathbf{I} - \nu_2\mathbf{L} \end{pmatrix}. \tag{B1}$$

The Laplacian is a real symmetric matrix; therefore, we can diagonalize it as $\mathbf{P}^T\mathbf{L}\mathbf{P} = \boldsymbol{\Lambda}$, where $\mathbf{P}$ is the matrix of the normalized eigenvectors of the Laplacian, that is, $P_{ij} = \frac{e^i_j}{\sqrt{N}}$ and $\mathbf{P}^T\mathbf{P} = \mathbf{I}$.

In a base defined by the transformation $\hat{\mathbf{P}}$,

$$\hat{\mathbf{P}} = \begin{pmatrix} \mathbf{P} & 0 \\ 0 & \mathbf{P} \end{pmatrix}, \tag{B2}$$

the matrix $\mathbf{A}$ becomes a block matrix of diagonal matrices:

$$\hat{\mathbf{A}} = \begin{pmatrix} a\mathbf{I} - \nu_1\boldsymbol{\Lambda} & b\mathbf{I} \\ c\mathbf{I} & d\mathbf{I} - \nu_2\boldsymbol{\Lambda} \end{pmatrix}. \tag{B3}$$

With this choice of base, the Lyapunov equation becomes equivalent to multiple algebraic systems (one for each eigenvalue of the Laplacian) and the solution is straightforward. Rotating the solution back to the original frame of reference gives Eq. (14) of the main manuscript.

APPENDIX C: NUMERICAL SIMULATIONS

This section provides details about the numerical simulations in order to replicate the results of the manuscript.

1. Scalar field simulation

The partial differential equation (PDE)

$$\frac{\partial u}{\partial t} = -u^3 - a\,u^2 + u\,(1 + a) + \mu\frac{\partial^2 u}{\partial x^2} + \sigma\xi \tag{C1}$$

was integrated for $u = u(t, x)$, with ξ being a Gaussian noise term decorrelated in time and space, that is, $\langle\xi(t, x)\xi(t', x')\rangle = \delta(x - x')\delta(t - t')$.

The integration was realized on a regular linear lattice of 1000 nodes for 100 000 time steps. A transient of 25 000 was discarded, then the time series was downsampled, keeping one time stamp every 100. The integration time, T, was related to the characteristic time, $\tau = \frac{1}{\lambda}$, as $T = 30\tau$, where λ has the same meaning as in the main manuscript. Finally, μ and the mesh spacing were chosen to fix the discrete diffusion coefficient to $\nu = 2$.

The integration was performed using the Euler-Maruyama method defining $\sigma = 0.005$.

2. 2D system simulation

As in the previous section, the PDEs,

$$\frac{\partial u}{\partial t} = au + bv + \mu_1\frac{\partial^2 u}{\partial x^2} + \sigma\xi_1, \tag{C2a}$$

$$\frac{\partial v}{\partial t} = cu + dv + \mu_2\frac{\partial^2 v}{\partial x^2} + \sigma\xi_2, \tag{C2b}$$

were integrated solving for $u = u(t, x)$ and $v = v(t, x)$ on a regular linear lattice of 1000 nodes for 100 000 time steps. A transient of 25 000 was discarded and then the time series was downsampled, keeping one time stamp every 100. The parameters μ_1, μ_2, and the lattice spacing were chosen such that the discrete diffusion coefficients are $\nu_1 = 4$ and $\nu_2 = 0.2$. The remaining parameters are $b = -c = -4$, and $d = 3/2$. The total integration time was chosen depending on the Jacobian matrix:

$$\mathbf{J} = \begin{pmatrix} a & b \\ c & d \end{pmatrix}. \tag{C3}$$

Defining $\bar{\lambda} = \max_i\{\lambda_i^J\}$, where λ_i^J is the spectrum of $\mathbf{J}$, the integration time was set as $T = 30/\bar{\lambda}$. The integration was performed using the Euler-Maruyama method setting $\sigma = 0.005$.

APPENDIX D: GENERIC DIFFUSIVE CONNECTIVITY

In the case of reaction-diffusion equations, the Laplacian of the discretized equations represents a regular lattice. Relaxing this assumption to consider a general connectivity matrix, the formalism can be extended to the study of networks of identical interacting units. In this case the inhomogeneities in the nodes' connectivities give rise to inhomogeneities in the covariance matrix, and the dynamic variables of the single nodes do not have the same distributions across nodes anymore.

In this case the spatial indicators based on neighbors become very hard to quantify analytically and, in general, would depend on the particular connectivity involved. Nevertheless, this limitation does not hold for the spatial variance, which can still be expressed in a closed form. Let us consider the system of interacting nodes:

$$\dot{u}_i = a u_i + b v_i - \alpha u_i^3 + \nu_1 \sum_{j\in\mathcal{N}_i} (u_j - u_i) + \sigma\xi_1, \quad \text{(D1a)}$$

$$\dot{v}_i = c u_i + d v_i - \alpha v_i^3 + \nu_2 \sum_{j\in\mathcal{N}_i} (v_j - v_i) + \sigma\xi_2, \quad \text{(D1b)}$$

where i is the node's index, and $\mathcal{N}_i$ represents the neighborhood of node i. The system has a fix point for $u_i = 0$, $v_i = 0$. The steady-state solution in the linearized limit of the Fokker-Plank equation will be a multivariate Gaussian of covariance $\mathbf{\Sigma}$ obtained by the solution of the continuous-time Lyapunov equation, as explained in the main text. The covariance matrix can be written as

$$\mathbf{\Sigma} = \begin{pmatrix} \mathbf{\Sigma}_{uu} & \mathbf{\Sigma}_{uv} \\ \mathbf{\Sigma}_{vu} & \mathbf{\Sigma}_{vv} \end{pmatrix}. \quad \text{(D2)}$$

The *spatial* variance of the field u at a certain time will be given by

$$\mathrm{VAR[u]} = \frac{1}{N}\sum_i^N u_i^2 = \frac{1}{N}\mathbf{u}^T\mathbf{u}, \quad \text{(D3)}$$

which is a sum of squares of normal variables of zero mean and covariance $\mathbf{\Sigma}_{uu}$. Its distribution can be determined writing $\mathbf{u} = \mathbf{\Sigma}_{uu}^{1/2}\mathbf{z}$, where $\mathbf{z}$ is a vector of normal variables of 0 mean and unitary variance. Therefore, $\mathrm{VAR[u]} = \frac{1}{N}\mathbf{z}^T\mathbf{\Sigma}_{uu}\mathbf{z}$. Since

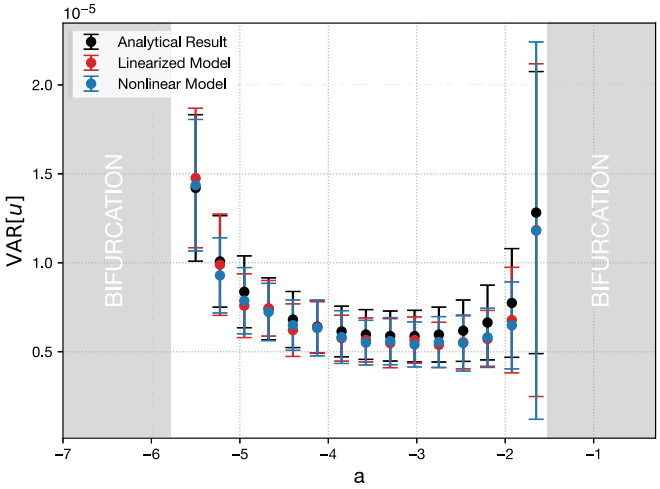

FIG. 5. Variance of the field u of Eq. (D1) for $N = 50$, $\nu_1 = 4$, $\nu_2 = 0.2$, $b = -c = -4$, $d = 3/2$, $\sigma = 0.005$, and different values of a. The connectivity between nodes is given by a random adjacency matrix of link density $\rho = 7.36\%$. Black: Analytical results, the filled dots represent the expected value while the error bars represent the standard deviation. Red: Simulations with $\alpha = 0$. Blue: Simulations with $\alpha = 1$. The dots represent the mean of the spatial variance computed across the simulation steps, while the error bars represent the standard deviation. The simulations were carried out for 100 000 steps using the Leimkuhler–Matthews method. A transient of 25 000 steps was discarded.

$\mathbf{\Sigma}_{uu}$ is symmetric and real, it can be diagonalized as $\mathbf{\Sigma}_{uu} = \mathbf{PDP}^T$. Since $\mathbf{P}$ is an orthogonal matrix, also the variable $\mathbf{w} = \mathbf{P^T z}$ is normal with unitary variance. Therefore,

$$\mathrm{VAR[u]} = \frac{1}{N}\mathbf{w}^T\mathbf{D}\mathbf{w} = \frac{1}{N}\sum_i^N \ell_i w_i^2, \quad \text{(D4)}$$

where ℓ_i are the eigenvalues of $\mathbf{\Sigma}_{uu}$. Hence, the variable $N\mathrm{VAR}[u]$ is a linear combination of N χ^2 variables of one degree of freedom. Such a variable is distributed according to the generalized χ-squared distribution and will have an expected value $E[N\mathrm{VAR}[u]] = \sum_i^N \ell_i = \mathrm{Tr}(\mathbf{\Sigma}_{uu})$ and variance $\mathrm{VAR}[N\mathrm{VAR}[u]] = 2\sum_i^N \ell_i^2$. We can finally note that the expected spatial variance is equivalent to the average of the temporal variance of the single u_i variables. This result is general and holds also in the case of a regular lattice. In Fig. 5 I report the result of the variable $\mathrm{VAR}[u]$ of the system given by Eq. (D2). A good agreement between the theory and the simulations can be observed.

[1] C. Kuehn, A mathematical framework for critical transitions: Bifurcations, fast–slow systems and stochastic dynamics, Physica D **240**, 1020 (2011).

[2] M. Scheffer, S. Carpenter, J. A. Foley, C. Folke, and B. Walker, Catastrophic shifts in ecosystems, Nature (London) **413**, 591 (2001).

[3] R. Biggs, S. R. Carpenter, and W. A. Brock, Turning back from the brink: Detecting an impending regime shift in time to avert it, Proc. Natl. Acad. Sci. USA **106**, 826 (2009).

[4] S. Kefi *et al.*, Spatial vegetation patterns and imminent desertification in Mediterranean arid ecosystems, Nature (London) **449**, 213 (2007).

[5] S. R. Carpenter, J. J. Cole, M. L. Pace, R. Batt, W. A. Brock, T. Cline, J. Coloso, J. R. Hodgson, J. F. Kitchell, D. A. Seekell *et al.*, Early warnings of regime shifts: A whole-ecosystem experiment, Science **332**, 1079 (2011).

[6] D. A. O'Brien, S. Deb, G. Gal, S. J. Thackeray, P. S. Dutta, S.-i. S. Matsuzaki, L. May, and C. F. Clements, Early warning

signals have limited applicability to empirical lake data, Nat. Commun. **14**, 7942 (2023).

[7] M. Scheffer, S. R. Carpenter, T. M. Lenton, J. Bascompte, W. Brock, V. Dakos, J. Van de Koppel, I. A. Van de Leemput, S. A. Levin, E. H. Van Nes *et al.*, Anticipating critical transitions, Science **338**, 344 (2012).

[8] J. M. Drake and B. D. Griffen, Early warning signals of extinction in deteriorating environments, Nature (London) **467**, 456 (2010).

[9] T. M. Lenton, Early warning of climate tipping points, Nat. Clim. Change **1**, 201 (2011).

[10] P. Ditlevsen and S. Ditlevsen, Warning of a forthcoming collapse of the Atlantic meridional overturning circulation, Nat. Commun. **14**, 4254 (2023).

[11] Y. Neuman, O. Nave, and E. Dolev, Buzzwords on their way to a tipping-point: A view from the blogosphere, Complexity **16**, 58 (2011).

[12] C. Diks, C. Hommes, and J. Wang, Critical slowing down as an early warning signal for financial crises? Empirical Econ. **57**, 1201 (2019).

[13] V. Dakos, E. Van Nes, R. Donangelo, H. Fort, and M. Scheffer, Spatial correlation as leading indicator of catastrophic shifts, Theor. Ecol. **3**, 163 (2010).

[14] V. Dakos, S. Kéfi, M. Rietkerk, E. H. Van Nes, and M. Scheffer, Slowing down in spatially patterned ecosystems at the brink of collapse, Am. Nat. **177**, E153 (2011).

[15] S. Kéfi, V. Guttal, W. A. Brock, S. R. Carpenter, A. M. Ellison, V. N. Livina, D. A. Seekell, M. Scheffer, E. H. Van Nes, and V. Dakos, Early warning signals of ecological transitions: Methods for spatial patterns, PLoS ONE **9**, e92097 (2014).

[16] S. Eby, A. Agrawal, S. Majumder, A. P. Dobson, and V. Guttal, Alternative stable states and spatial indicators of critical slowing down along a spatial gradient in a savanna ecosystem, Global Ecol. Biogeogr. **26**, 638 (2017).

[17] V. Dakos, E. H. Van Nes, P. d'Odorico, and M. Scheffer, Robustness of variance and autocorrelation as indicators of critical slowing down, Ecology **93**, 264 (2012).

[18] V. Guttal and C. Jayaprakash, Spatial variance and spatial skewness: Leading indicators of regime shifts in spatial ecological systems, Theor. Ecol. **2**, 3 (2009).

[19] M. P. Veldhuis, R. Martinez-Garcia, V. Deblauwe, and V. Dakos, Remotely-sensed slowing down in spatially patterned dryland ecosystems, Ecography **2022**, e06139 (2022).

[20] G. Tirabassi and C. Masoller, Entropy-based early detection of critical transitions in spatial vegetation fields, Proc. Natl. Acad. Sci. USA **120**, e2215667120 (2023).

[21] N. M. Shnerb, P. Sarah, H. Lavee, and S. Solomon, Reactive glass and vegetation patterns, Phys. Rev. Lett. **90**, 038101 (2003).

[22] R. HilleRisLambers, M. Rietkerk, F. van den Bosch, H. H. Prins, and H. de Kroon, Vegetation pattern formation in semiarid grazing systems, Ecology **82**, 50 (2001).

[23] C. W. Gardiner *et al.*, *Handbook of Stochastic Methods* (Springer, Berlin, 1985), Vol. 3.

[24] P. Davis, *Circulant Matrices*, Monographs and Textbooks in Pure and Applied Mathematics (Wiley, New York, 1979).

[25] H. V. Ribeiro, L. Zunino, E. K. Lenzi, P. A. Santoro, and R. S. Mendes, Complexity-entropy causality plane as a complexity measure for two-dimensional patterns, PLoS ONE **7**, e40689 (2012).

[26] K. Keller and H. Lauffer, Symbolic analysis of high-dimensional time series, Int. J. Bifurcation Chaos **13**, 2657 (2003).

[27] H. Fort and T. S. Grigera, A new early warning indicator of tree species crashes from effective intraspecific interactions in tropical forests, Ecol. Indic. **125**, 107506 (2021).

[28] C. Bandt and B. Pompe, Permutation entropy: A natural complexity measure for time series, Phys. Rev. Lett. **88**, 174102 (2002).